Journal of Molecular Spectroscopy 328 (2016) 37–45

Contents lists available at ScienceDirect

Journal of Molecular Spectroscopy

journal homepage: www.elsevier.com/locate/jms

Predicting accurate fluorescent spectra for high molecular weight polycyclic aromatic hydrocarbons using density functional theory

Jacob Powell, Emily C. Heider, Andres Campiglia, James K. Harper *

Department of Chemistry, University of Central Florida, 4111 Libra Drive, Orlando, FL 32816, United States

ARTICLE INFO

Article history:
Received 14 May 2016
In revised form 15 June 2016
Accepted 30 June 2016
Available online 9 July 2016

Keywords:
Polycyclic aromatic hydrocarbons
Shpol'skii
Fluorescence
Density functional theory
Polarized continuum model

ABSTRACT

The ability of density functional theory (DFT) methods to predict accurate fluorescence spectra for polycyclic aromatic hydrocarbons (PAHs) is explored. Two methods, PBE0 and CAM-B3LYP, are evaluated both in the gas phase and in solution. Spectra for several of the most toxic PAHs are predicted and compared to experiment, including three isomers of $C_{24}H_{14}$ and a PAH containing heteroatoms. Unusually high-resolution experimental spectra are obtained for comparison by analyzing each PAH at 4.2 K in an *n*-alkane matrix. All theoretical spectra visually conform to the profiles of the experimental data but are systematically offset by a small amount. Specifically, when solvent is included the PBE0 functional overestimates peaks by 16.1 ± 6.6 nm while CAM-B3LYP underestimates the same transitions by 14.5 ± 7.6 nm. These calculated spectra can be empirically corrected to decrease the uncertainties to 6.5 ± 5.1 and 5.7 ± 5.1 nm for the PBE0 and CAM-B3LYP methods, respectively. A comparison of computed spectra in the gas phase indicates that the inclusion of *n*-octane shifts peaks by +11 nm on average and this change is roughly equivalent for PBE0 and CAM-B3LYP. An automated approach for comparing spectra is also described that minimizes residuals between a given theoretical spectrum and all available experimental spectra. This approach identifies the correct spectrum in all cases and excludes approximately 80% of the incorrect spectra, demonstrating that an automated search of theoretical libraries of spectra may eventually become feasible.

1. Introduction

Polycyclic aromatic hydrocarbons (PAHs) are compounds composed of two or more aromatic rings containing only carbon and hydrogen. These products are found in meteors [1], interplanetary dust particles [2], and interstellar grains [3]. In our terrestrial environment, PAHs often occur as products of incomplete combustion. PAHs formed by the birth of stars are ubiquitous in nature, and pose great interest in a variety of fields – from measuring the rate of star formation [4] to possible uses as semiconductors [5]. While the presence of PAHs in space inspires studies into the origin of biological molecules and mechanism for PAH growth [6], in Earth's ecosystem real concerns exist regarding the interaction of PAHs with biomolecules. Epidemiological studies have revealed high toxicity and carcinogenicity for many of these compounds and sixteen are now included on the Environmental Protection Agencies (EPA) list of Priority Pollutants for routine monitoring. Anthropogenic sources of PAHs include wood and coal burning, and their presence in coal and crude oil insures their extraction from the ground and potential for distribution. These factors make PAHs one of the most omnipresent pollutants worldwide. Developing sensitive methods to quantify and identify PAHs in air, water, and soil are therefore of critical importance.

While remote detection of PAHs has revolved around measured and calculated vibrational spectra [7], work in the Campiglia laboratory and by others has [8] exploited the fluorescence [9] and phosphorescence [10] emission of PAHs to quantify and identify PAHs in terrestrial environmental samples including water [11] and soil [12]. The use of luminescence provides several advantages over vibrational spectroscopy including improved sensitivity and specificity with fluorescence detection of PAHs routinely providing part-per-trillion limits of detection. Specificity in fluorescence can be further enhanced with time resolved line-narrowing spectroscopy. This process involves diluting PAH samples in solvents with minimal solute interaction (generally *n*-alkane solvents) then freezing to cryogenic temperatures (liquid nitrogen or helium) to produce vibrationally resolved fluorescence emission spectra with sufficient resolution to identify individual vibronic transitions. This cryogenic technique is generally referred to as Shpol'skii spectroscopy [13]. Additional specificity can be attained with the measurement of fluorescence lifetimes [14].

* Corresponding author.
E-mail address: james.harper@ucf.edu (J.K. Harper).

http://dx.doi.org/10.1016/j.jms.2016.06.015
0022-2852/

In previous work, we have measured Shpol'skii spectra for several of the EPA PAHs and most have been found to exhibit unique spectra [11,12]. These significant differences between spectra mean that complex mixtures of PAHs (e.g. environmental samples) can potentially be characterized. Moreover, since at least some unique emission frequencies are observed for most PAHs, analysis of mixtures is possible without prior chromatographic separation in analyses requiring only a few minutes [15]. Recently, this methodology has been employed to successfully characterize multiple PAHs in complex mixtures available as "reference materials" from the National Institute of Standards and Technology (NIST) [15]. One of the challenges identified in these studies was the discovery that many of the samples contained emission peaks at frequencies not associated with any of the 16 EPA-PAH standards. This is not surprising as the EPA-PAHs are only a small fraction of the total number of PAHs known to exist in environmental samples. Further limiting the monitoring of environmental PAHs is the modest commercial availability of certain pure standards. Many cases also exist where the cost of pure PAH standards is prohibitive. This is particularly true for dibenzopyrene isomers with molecular weight 302. Several dibenzopyrenes are more toxic than benzo[*a*]pyrene, which is the most toxic PAH in the EPA priority pollutants list [16]. Synthesis is always an alternative to overcome the lack of commercial standards. Unfortunately, the existence of numerous isomers with the same molecular weight and very similar molecular structures often challenges the synthesis and purification of individual standards.

Very recently a new alternative to synthesis has become available for identifying PHAs when standards are unavailable. This approach relies on theoretical methods to calculate vibrationally resolved emission spectra for candidate structures [17]. Historically, accurate descriptions of electronic excited states were difficult to obtain because conventional density functional theory (DFT), i.e. Hohenberg-Kohn, was limited to ground states [18]. The development of time-dependent DFT (TDDFT) [19] extends conventional DFT to excited states and allows for studies of emission spectra. A second obstacle arose from the large number of excited vibrational states that must be evaluated in all but the smallest molecules. A key breakthrough in treating these transitions came from the recognition that the majority of the possible vibronic transitions do not, in fact, contribute to the spectrum. A set of rules has recently been developed to identify non-negligible transitions, allowing calculations to be restricted to only these levels [20]. This development has led to a powerful process for computing DFT emission spectra in larger molecules and a more complete description of this approach is given elsewhere [17]. This methodology allows the influence of temperature and a wide range of solvents to be included. Perhaps most significantly, this computational methodology has now been implemented into the widely available computational package, Gaussian, and results in a facile prediction process that non-experts can employ to effectively predict spectra in larger molecules. These techniques have the potential to provide a unique path to structure of higher molecular weight PAHs in environmental samples.

At the present time, these computational methods have been employed to predict spectra for several fluorescent molecules [21], but less has been done to evaluate the accuracy of these methods when computing emission spectra for PAHs. To our knowledge, computational methods have been employed to study a total of 15 PAHs [20a,22] and 3 of these have included solvent effects. Of the predicted spectra, 8 involve PAHs on the EPA list and most have molecular weights of 228 or less. Here, one major aim is to evaluate the ability of these DFT methods to calculate accurate emission spectra for higher molecular weight PAHs in a manner that includes solvent effects. A secondary objective is to develop methods for comparing these predicted spectra to unusually high-resolution experimental data obtained at 4.2 K with the aim of consistently identifying the correct PAHs based on statistical figures-of-merit. Compounds selected for analysis are shown in Fig. 1 and include benzo[*a*]pyrene, dibenzo[*a,l*]pyrene, dibenzo[*a,e*]pyrene, dibenzo[*a,i*]pyrene, and (−)-7R,8S,9R,10S-7,8,9,10-tetrahydroxy-7,8,9,10-tetrahydrobenzo[*a*]pyrene (referred to hereinafter as "benzo[*a*]pyrene tetrol"). Benzo[*a*]pyrene was selected for analysis because it is one of the most toxic compounds on the EPA list [23]. However, dibenzo[*a,l*]pyrene and dibenzo[*a,i*]pyrene are estimated to be roughly 10 times more toxic that benzo[*a*]pyrene while dibenzo[*a,e*]pyrene is considered equivalent in toxicity to benzo[*a*]pyrene [24]. Currently, however, none of these dibenzopyrenes are included on the EPA list. Since these compounds are presently recommended for monitoring in the European Union [24] and may be monitored by the EPA in the future, they were also studied here. The inclusion of the three dibenzopyrene isomers is also significant because it allows for a rigorous evaluation of the DFT methods' ability to distinguish structurally similar isomers. Likewise, benzo[*a*]pyrene tetrol tests the ability of the theoretical methods to predict spectra of polycyclic aromatic compound with heteroatoms (e.g. O or S) in their molecular structure. Benzo[*a*]pyrene-7,8,9,10-tetrol is a well-known metabolic product of benzo[*a*]pyrene often used as a biomarker of human exposure to PAHs [25].

In the following discussion, two theoretical methods, PBE0 [26] and CAM-B3LYP [27], are evaluated for their ability to accurately reproduce experimental spectra. Because each of these methods is found to exhibit systematic errors, an empirical correction is introduced. These adjusted theoretical spectra are ultimately compared to experimental data using a process that minimizes residuals. The correct experimental spectrum is found to match the predicted spectra in all cases and the majority of the incorrect spectra are eliminated as possible matches. All spectra are computed in an environment that simulates solvent and in all cases

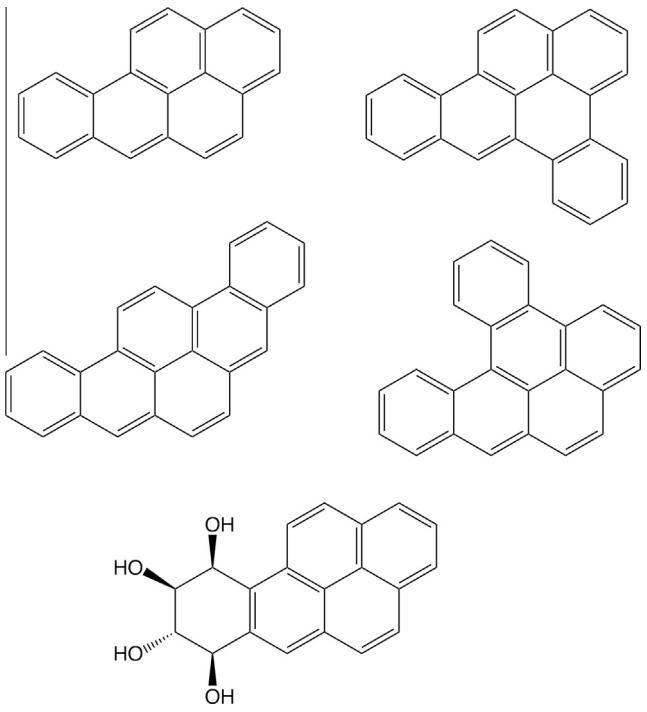

Fig. 1. Structures studied herein include benzo[*a*]pyrene (top left), dibenzo[*a,e*]pyrene (top right), dibenzo[*a,i*]pyrene (middle left), dibenzo[*a,l*]pyrene (middle right) and Benzo[*a*]pyrene–7,8,9,10-tetrol (bottom).

the solvent is found to shift the spectrum to higher wavelengths by 10–26 nm.

2. Experimental

Nanopure water from a Barnstead Nanopure Infinity water system was used throughout. HPLC grade *n*-octane was purchased from Acros Organics (Atlanta, GA). Benzo[*a*]pyrene, dibenzo[*a,e*]pyrene, dibenzo[*a,i*]pyrene and dibenzo[*a,l*]pyrene were purchased from AccuStandard at their highest available purity (100%). benzo[*a*]pyrene–7,8,9,10-tetrol was obtained from the NCI Chemical Carcinogen Repository, Midwest Research Institute (Kansas City, MO). Note: use extreme caution when handling PAHs as many are known to be extremely toxic.

Stock solutions of all PAHs were prepared in *n*-octane and kept in the dark at 4 °C. Possible PAH degradation was monitored via room-temperature fluorescence (RTF) spectroscopy. Working solutions of PAHs were prepared by serial dilution of their stock solutions with *n*-octane.

All room temperature steady-state excitation and fluorescence spectra were acquired with a commercial spectrofluorimeter (Photon Technology International). The excitation source was a continuous wave 75-W xenon lamp with broadband illumination from 200 to 2000 nm. The excitation and emission monochromator had the same reciprocal linear dispersion (4 nm mm^{-1}), accuracy (±1 nm), reproducibility (±2 nm) and spectral resolution (0.25 nm). Both monochromators have 100 grooves/nm gratings blazed at 300 and 400 nm, respectively. Detection was made with a photomultiplier tube (model 1527) with spectral response from 185 to 650 nm. In the photon counting mode, the maximum count rate was 4 MHz, rise time 20 ns and fall time 100 ns with a 220 ns pulse width. The instrument was computer controlled using commercial software (Felix32) specifically designed for the system. Excitation and emission spectra were corrected for wavelength dependence of excitation light source and detector sensitivity, respectively. Correction was made in the post-acquisition mode using the radiometric correction factors included in Felix32 software. Long pass filters were used when necessary to eliminate second-order emission from the excitation source. Instrumental performance was monitored with a commercial standard (Photon Technology International) consisting of a single crystal of dysprosium-activated yttrium aluminum garnet mounted in a cuvette-sized holder with a well-characterized quasi-line excitation and emission spectrum. Wavelength accuracy and precision was evaluated periodically by comparing the recorded position of several excitation and emission spectral lines obtained from repetitive scans within 250–800 nm to the maximum excitation and emission wavelengths provided by the manufacturer. Room-temperature measurements were made from un-degassed solutions with a standard 600 μL quartz cuvettes with a 1 cm cell path. A 90° excitation/emission configuration was used in all measurements.

The 4.2 K measurements were carried out with the aid of a cryogenic fiber optic probe [9]. The probe consisted of one delivery and six collection fibers. All fibers were 3 m-long and 500-μm-core-diameter, silica-clad silica with polyimide buffer coating (Polymicro Technologies, Inc.). The fibers were fed into a 1.2-m-long section of copper tubing that provided mechanical support for lowering the probe into the liquid helium. At the sample end, the fibers were arranged in a conventional six-around-one configuration with the delivery fiber in the center, bundled with vacuum epoxy (Torr-Seal, Varian Products), fed into a metal sleeve, and aligned with the entrance slit of the spectrometer. The dimensions of the vial were the following: 30-mm length, 5.5-mm inner diameter, and 7-mm outer diameter. Its maximum volume capacity was 750 μL. The measurement procedure was as follows: after transferring a known volume (typically 100–200 μL) of un-degassed sample solution with a pipette into the sample vial of the cryogenic probe, the tip of the fiber-optic bundle was positioned and held constant with the screw cap above the solution surface. Sample freezing was accomplished by lowering the copper tubing into the liquid helium, which was held in a Dewar with 60 L storage capacity. The liquid helium would typically last three weeks of daily use, averaging 15–20 samples per day. Complete sample freezing took less than 90 s per sample. Replacing the frozen sample involved removing the sample vial from the cryogen container and melting the frozen sample with a heat gun. Because no physical contact between the tip of the fiber-optic bundle and the sample ever occurred during measurements, probe clean up between measurements was not necessary. The entire freeze, thaw, and sample replacement cycle took no longer than 5 min.

All Shpol'skii spectroscopy (LETRSS) Measurements were carried out with a multidimensional luminescence system built in our lab. Its complete description and full measuring capabilities – i.e. for absorption, excitation, fluorescence and phosphorescence measurements – have been reported previously [28]. The system was operated in the external trigger mode. Data acquisition parameters (gate delay and gate width) were entered on the control computer with Andor software and the appropriate control signals were sent via a GPIB interface to the pulse generator. Once triggered by the laser, the pulse generator used this information to determine when the image intensifier in the detector head was gated on (gate delay) and for how long it was gated on (gate width). When the intensifier was gated off, the acquired data were transferred from the detector head to the controller card (32-bit Intelligent Bus-Mastering PCI card) in the computer. Complete instrument control was carried out with LabView (National Instruments, version 6.0) based software developed in our lab.

Fluorescence spectra were recorded using a minimum delay of 10 ns, which was sufficient to avoid the need to consider convolution of the laser pulse with the analytical signal. The measuring gate was optimized to collect most of PAH fluorescence and still avoid instrumental noise. Unless otherwise noted, each spectrum corresponds to the accumulation of 100 laser pulses. The limiting resolution for recording excitation spectra was dictated by the minimum scanning rate of the tunable dye laser, namely 0.1 nm/data point. The best resolution for recording fluorescence spectra was dictated by the limiting resolution of the spectrograph/ICCD system, which corresponded to 0.32–0.40 nm [28].

For computations of theoretical spectra, all geometry optimizations and frequency calculations in both the ground state and excited state were calculated using the functionals CAM-B3LYP [27] and PBE0 [26] together with the cc-pVDZ basis set [29]. Fluorescence emission spectra were calculated using the Franck-Condon approximation [17a,17c]. The polarizable continuum model (PCM) [30] was used to simulate solvent effects. All calculations were performed using the Gaussian 09 software package [31].

3. Results and discussion

3.1. Experimental fluorescence spectra at room temperature and 4.2 K

Experimental Shpol'skii emission spectra were acquired for each of the 5 PAHs studied herein. Pure standards were diluted in *n*-octane to 100 ng mL^{-1} (ppb) then frozen in liquid helium (ca. 4.2 K). For comparison, emission spectra were also acquired for each PAH at room temperature (ca. 278 K) in *n*-octane using a conventional fluorometer (Fig. 2). A 3/3 nm excitation/emission band-pass was needed at room temperature to obtain an acceptable signal-to-noise ratio from all the studied compounds. Lower-

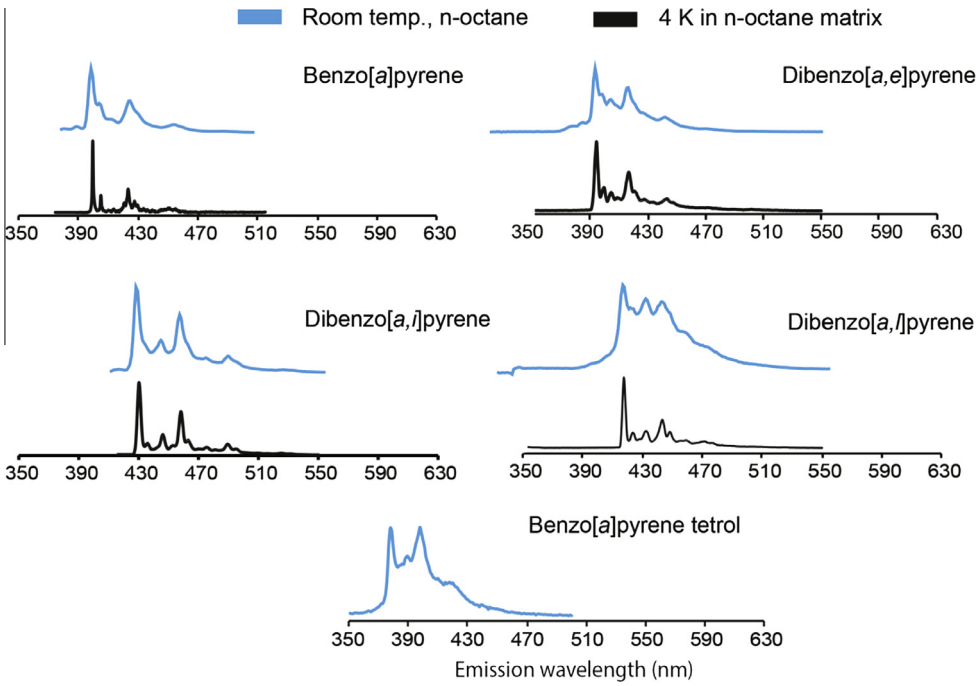

Fig. 2. Fluorescence spectra for the PAHs studied here. In each plot, the top spectrum (blue) is obtained in *n*-octane at room temperature while the bottom spectrum (black) represents the same sample after cryogenic freezing in liquid helium. All Shpol'skii spectra were recorded under site-selective excitation (λ_{exc}) at the following wavelengths: λ_{exc} = 298.0 nm (benzo[*a*]pyrene), λ_{exc} = 306.4 nm (dibenzo[*a,e*]pyrene), λ_{exc} = 312.0 nm (dibenzo[*a,i*]pyrene) and λ_{exc} = 318.0 nm (dibenzo[*a,l*]pyrene). No Shpol'skii spectrum was acquired for benzo[*a*]pyrene tetrol, thus only the solution spectrum in methanol is displayed. (For interpretation of the references to color in this figure legend, the reader is referred to the web version of this article.)

ing the temperature to 4.2 K enhanced the fluorescence intensities of the studied PAHs. The low temperature data was then recorded using a 1/1 nm excitation/emission band-pass. The room-temperature fluorescence spectra show typical vibrational structures often observed from PAHs in liquid solutions. The same is true for the room temperature fluorescence spectrum of benzo[*a*]pyrene tetrol. The 4.2 K spectral features of the PAHs show the quasi-line structure usually observed from Shpol'skii systems. The broad, featureless fluorescence bands we observed were due to molecules freezing out from the crystalline phase into the amorphous phase at the point of matrix solidification. The low solubility of benzo[*a*]pyrene tetrol in *n*-octane prevented us from recording quasi-line fluorescence spectra at 4.2 K.

Close examination of 4.2 K data shows characteristic fluorescence profiles for all the studied PAHs. The maximum fluorescence peaks correspond to the $S_{1,0} \rightarrow S_{0,0}$ transition and reveal significant wavelength differences for isomers of the same molecular weight. The same is true for the fluorescence maximum of benzo[*a*]pyrene. The spectral fingerprints of PAHs in Shpol'skii matrixes make possible their direct determination in complex samples without previous chromatographic separation [11,12,14].

3.2. Predicting fluorescence spectra with PBE0 and CAM-B3LYP

In this study, a key question is whether theoretical methods can accurately reproduce experimental Shpol'skii spectra for PAHs of environmental importance. Here, two methods were evaluated, namely PBE0 and CAM-B3LYP. The PBE0 approach was employed initially because it has been found to give reasonably accurate emission spectra in previous studies [32]. Here, *n*-octane was included as a solvent using the polarized continuum model [30]. A more detailed description of the computational process utilized is given in Section 2. It is noteworthy that Shpol'skii spectra are obtained when the solvent is present as a solid, thus one of the aims of this study is to see if a computational solvent model can be used to accurately represent the solid. Predicted spectra for the 5 model PAHs from PBE0 in *n*-octane are shown in Fig. 3, together with experimental Shpol'skii data.

In all cases, the computed PBE0 spectra exhibit the majority of the lines observed experimentally. The relative peak intensities are also largely consistent with experiment but there are notable differences, such as the overestimation of peak intensities for the peak corresponding to those near 460 nm in the experimental spectrum of dibenzo[*a,i*]pyrene. Perhaps more significantly, all predicted spectra also exhibit a systematic error involving an overestimation of the emission wavelengths by an average of 16.1 ± 6.6 nm based upon the position of the $S_{1,0} \rightarrow S_{0,0}$ transitions. A second type of error is also present in which all PBE0 calculated spectral lines occupy an expanded wavelength range approximately 29% larger, on average, than those in the corresponding experimental spectra.

The errors observed in the PBE0 computations suggest that other theoretical methods may be more suitable for analyzing PAH emission spectra. Recently, the CAM-B3LYP method has been introduced to include long-range corrections and this method has been found to provide accurate emission spectra for some compounds. Accordingly, spectra for the 5 model compounds were calculated at the CAM-B3LYP/cc-pVDZ level of theory. All spectra are illustrated in Fig. 4.

Spectra predicted by the CAM-B3LYP method accurately reproduce most experimental lines. The relative peak intensities mimics those observed experimentally, but there are notable regions where over/underestimations of intensities are present. These spectra also exhibit a more significant systematic error in which all emission wavelengths are underestimated by 14.5 ± 7.6 nm based upon the position of the $S_{1,0} \rightarrow S_{0,0}$ transitions. Notably, these CAM-B3LYP spectra also contain the second type of error noted for the PBE0 calculated spectra in which the range of

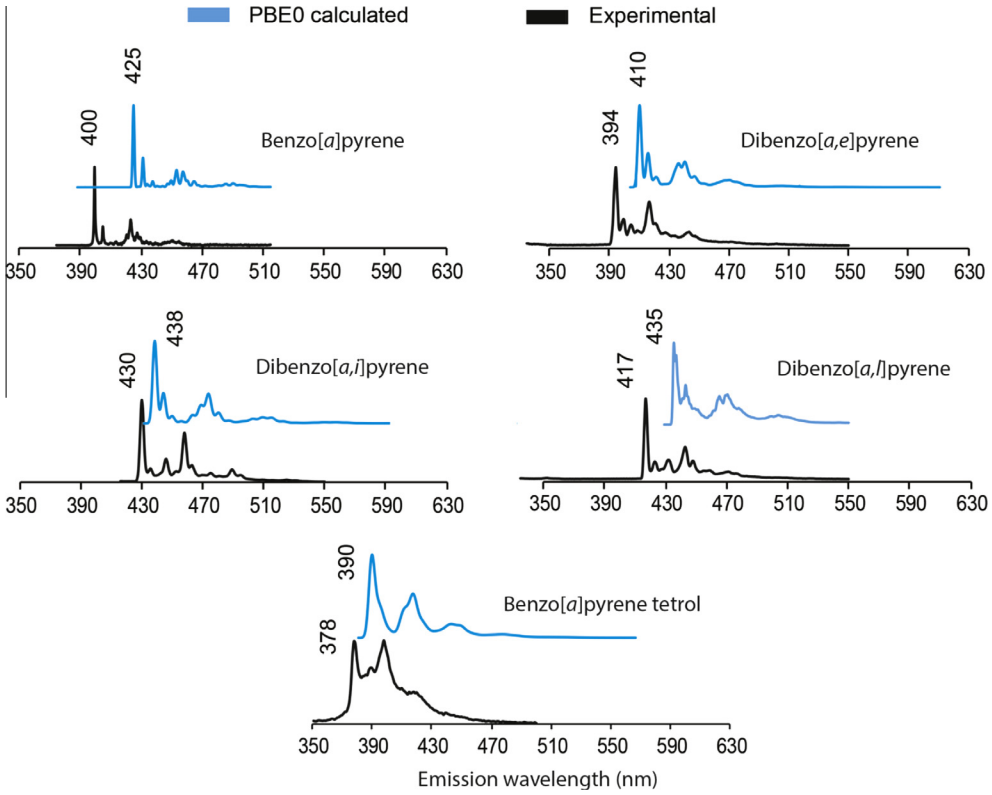

Fig. 3. A comparison of experimental fluorescence spectra (black) in an *n*-octane matrix and calculated spectra (blue). The experimental spectrum for benzo[*a*]pyrene tetrol was acquired at room temperature in methanol. Theoretical spectra are calculated at the PBE0/cc-pVDZ level of theory and include *n*-octane or methanol as a solvent. The wavelength of the $S_{1,0} \rightarrow S_{0,0}$ transition is marked in both experimental and computed spectra. (For interpretation of the references to color in this figure legend, the reader is referred to the web version of this article.)

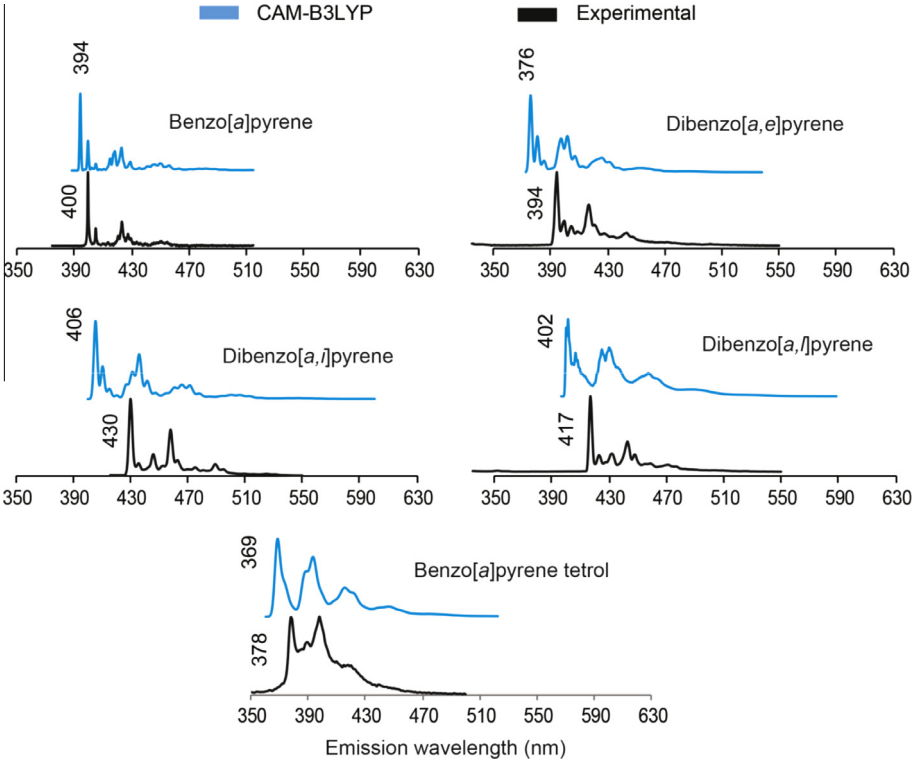

Fig. 4. A comparison of experimental emission spectra (black) and calculated spectra (blue). Theoretical spectra are obtained at the CAM-B3LYP/cc-pVDZ level of theory and include *n*-octane or methanol as a solvent. The wavelength of the $S_{1,0} \rightarrow S_{0,0}$ transition is indicated in both experimental and computed spectra. (For interpretation of the references to color in this figure legend, the reader is referred to the web version of this article.)

wavelengths predicted was approximately 16% larger on average than that found in experimental spectra. Both kinds of systematic errors are smaller in CAM-B3LYP spectra than in PBE0. One notable difference between CAM-B3LYP and PBE0 is that CAM-B3LYP more accurately predicts the peak intensities for peaks that occur at wavelengths higher than the $S_{1,0} \rightarrow S_{0,0}$ transitions. Taken together, these results indicate that the CAM-B3LYP functional provides more accurate spectra for the PAHs studied here.

3.3. Improving comparisons between predicted and experimental spectra

The ability of the PBE0 and CAM-B3LYP methods to reproduce experimental fluorescence spectra with reasonable accuracy demonstrates that theoretical spectra can potentially be employed to evaluate experimental results. It is, however, desirable to minimize the systematic errors identified above before comparing these DFT spectra. Here, an empirical approach was explored as a way to further improve the match between experimental and computed spectra. It is observed that a plot of the wavelengths of all major experimental lines versus the corresponding wavelengths in computed spectra are linearly correlated (Fig. 5). A least-squares fit to the data gave the relationships listed in Table 1.

These empirical relationships partially correct the over or underestimation of peak positions and also contract the spectral range over which peaks are predicted to occur to more closely match experimental data. This approach has been used extensively in comparing calculated and experimental NMR data [33]. All computed spectra were adjusted using these relationships and the resulting spectra are shown in Fig. 6. Because there is a scatter in the data of Fig. 5, this adjustment is an *average* correction and the fit in any given individual case, while significantly improved, can be slightly high or low.

After the empirical correction the average difference between theory and experiment is 6.5 ± 5.1 nm and 5.7 ± 5.1 nm, respectively for PBE0 and CAM-B3LYP based upon the position of the $S_{1,0} \rightarrow S_{0,0}$ transitions.

An important consideration in this study is whether calculated spectra are sufficiently accurate to match *only* the correct experimental spectrum. Here an initial test was performed comparing a given theoretical spectrum with each of the 5 experimental spectra. For each pair of spectra compared, a residual was computed (see Section 2) and this figure-of-merit provided a means to select among the different PAHs. Because any theoretical spectrum can be slightly offset from experimental data, an adjustment is typically needed to obtain the optimal fit. To make this adjustment process independent of an operator, and thus less biased, a computer controlled process was developed, involving a series of adjustments in which the entire theoretical spectrum was moved in increments of ±0.5 nm and a residual computed at each point. For any given compound, this process creates a group of residuals; one for each offset value. A best fit is taken as the adjustment providing a minimum in the residuals. This process also serves to identify other experimental PAHs fitting a theoretical spectrum. These adjustments are restricted to a small region of the spectrum corresponding to ±3σ (i.e. the uncertainty in the computed spectra) where σ = ±5.7 nm for CAM-B3LYP and ±6.5 nm for PBE0. The Python code used herein for these adjustments is provided as Supplemental Information. An example of the type of output created is illustrated in Fig. 7 for dibenzo[*a,e*]pyrene. Ideally, only a single experimental spectrum will match a computed spectrum, allowing unambiguous identification of the PAH. In the case of the five PAH studied here, all theoretical spectra were found to match the correct experimental data. In addition, however, four of the compounds evaluated also matched one other experimental spectrum. Only dibenzo[*a,e*]pyrene exclusively matched the correct experimental spectrum and the adjusted spectrum is illustrated in Fig. 8. A summary of the PAHs matching a given theoretical spectrum is provided in Table 2.

Overall, the approach of minimizing residuals provided a match to the correct experimental spectra in all cases and eliminated 80% of the incorrect matches with high statistical confidence (i.e. 95%). This methodology is, admittedly, somewhat limited and was employed only to explore the feasibility of using theoretical spectra to improve analysis of experimental emission spectra. We note that significantly more selective analysis techniques are widely available [34] and, in future studies, will likely improve the ability to match a given experimental spectrum.

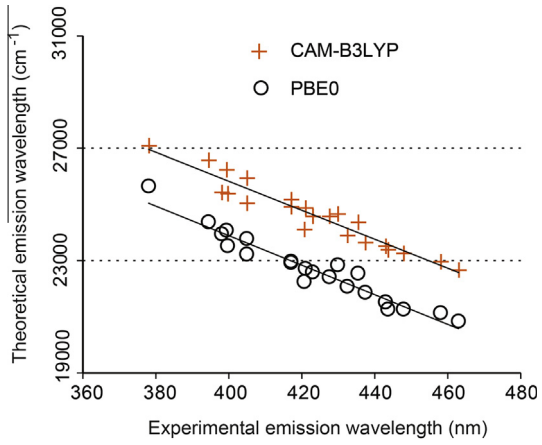

Fig. 5. A plot of experimental emission wavelengths for all major peaks in the 5 PAH samples studied versus the corresponding peaks in theoretical spectra. Computed spectra and are strongly correlated with experimental data with respective R^2 values of 0.925 and 0.932, respectively, for PBE0 and CAM-B3LYP.

Table 1
Linear correlations relating computed and experimental emission spectra.

Method	Relationship	R^2
PBE0	$\lambda_{cm^{-1}}^{Calculated} = -52.94\lambda_{nm}^{Experimental} + 45,069$	0.925
CAM-B3LYP	$\lambda_{cm^{-1}}^{Calculated} = -51.81\lambda_{nm}^{Experimental} + 46,539$	0.932

3.4. The influence of solvent on calculated spectra

All calculations described here included a solvent in the model with the solvent employed being either methanol (for benzo[*a*]pyrene tetrol) or *n*-octane (for PAHs containing only C and H). Solvents should be included in fluorescence predictions because the local environment has a strong influence on fluorescence properties. In the present study, this environment involves a solvent that is present as a solid at 4.2 K. Because the solvent in Shpol'skii spectroscopy is selected to have minimal interactions with the PAH, a solvent model that accurately described the polarization of the neighboring regions was considered an ideal choice. Accordingly, the polarized continuum model (PCM) was selected since it correctly describes the average polarization of the environment without including specific solvent effects such as strongly hydrogen-bonded moieties. In general, it is possible to include such specific interactions by including clusters of solvent molecules within the PCM, but in the case of PAHs this was considered unnecessary.

For the PAHs studied here, the inclusion of *n*-octane was found to move all peaks to lower energies (i.e. higher wavelengths) and to influence all peaks in a spectrum equally. A plot showing computed spectra with and without a solvent model is given in Fig. 9. Those PAHs containing only C and H exhibited nearly the

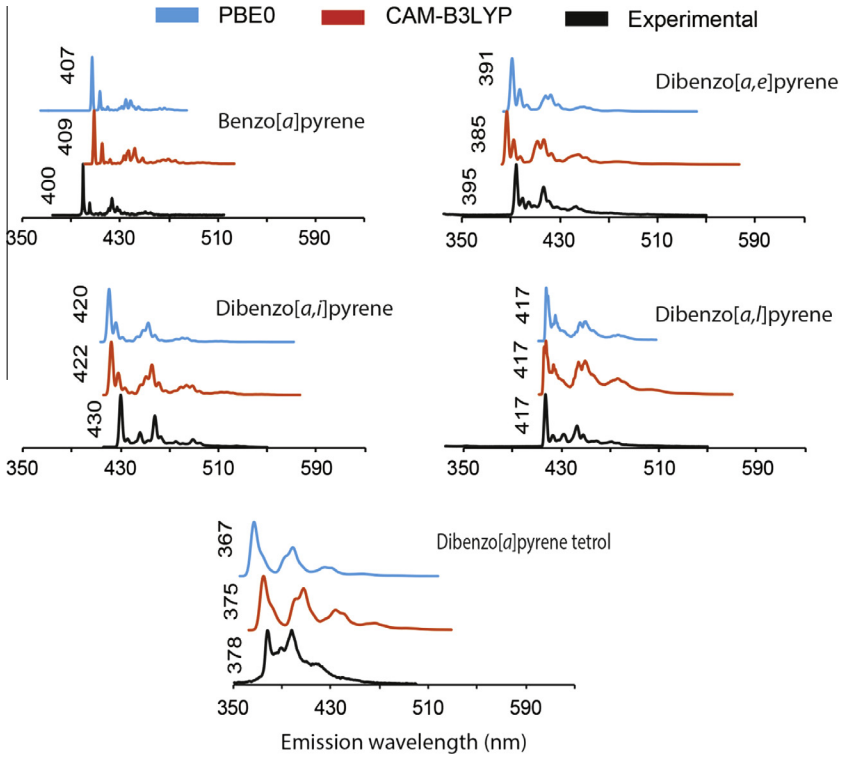

Fig. 6. A comparison of calculated and experimental fluorescence spectra. All computed spectra have been adjusted to correct for systematic over or underestimations in wavelengths and overestimations in the range of wavelengths over which the transitions occur. Computed spectra from the PBE0 and CAM-B3LYP methods are represented, respectively, by blue and orange plots. (For interpretation of the references to color in this figure legend, the reader is referred to the web version of this article.)

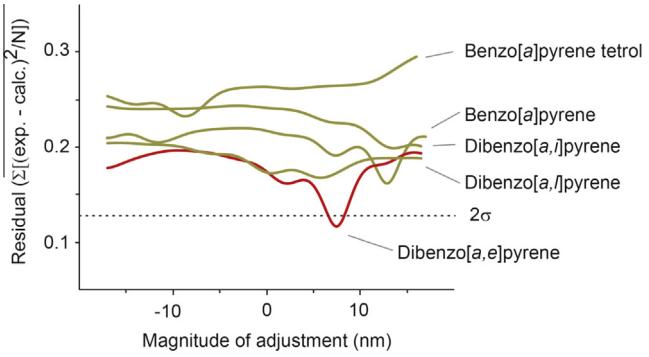

Fig. 7. Residuals derived from a comparison of the theoretical spectrum of dibenzo[a,e] pyrene with experimental data from the 5 PAHs studies herein. Only the experimental spectrum of dibenzo[a,e]pyrene matches this theoretical data, demonstrating that accurate vibronic spectra can be computed using DFT methods.

same change with CAM-B3LYP shifting the peaks by +11.1 ± 2.8 nm and PBE0 altering the peaks by +10.6 ± 3.1 nm. Because CAM-B3LYP underestimates the wavelength of the transitions, the addition of solvent significantly improves the fit to experimental data. In contrast, PBE0 overestimates these wavelengths, thus solvent inclusion further deteriorates the match with experimental data. It is interesting to note that while benzo[a]pyrene tetrol also shows a shift of the peaks to larger wavelengths upon solvent inclusion (MeOH), the effect is roughly 2.6 time larger (i.e. +26.2 ± 0.2 nm) than that observed in unsubstituted PAHs. Including solvent also provides a better match between the relative intensity of the peaks computed for benzo[a]pyrene tetrol and experimental data.

Overall these data comparing gas and solvent effects indicate that the PCM model accurately represents a solvent and that including the influence of solvent becomes more important as the polarity of the PAH increases.

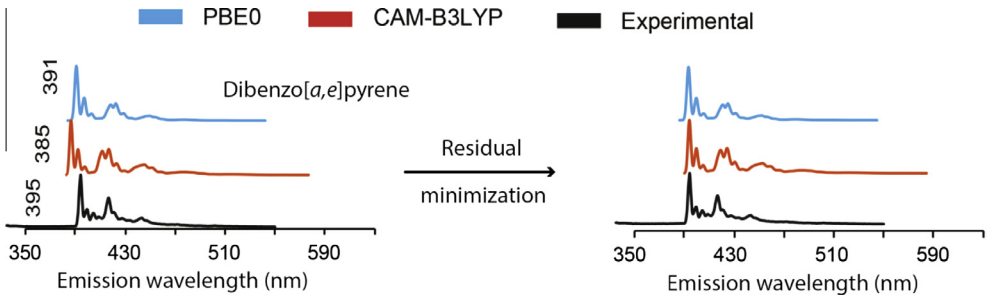

Fig. 8. A comparison of the DFT predicted spectra for dibenzo[a,e]pyrene before (left) and after (right) adjusting the theoretical spectra to minimize the residuals. The initial theoretical spectra (left) have previously been partially adjusted utilizing the empirical correction described in the text.

Table 2
Experimental spectra matching calculated DFT spectra.

PAH	Possible matches[a]
Benzo[*a*]pyrene	Benzo[*a*]pyrene, Dibenzo[*a,l*]pyrene
Dibenzo[*a,l*]pyrene	Dibenzo[*a,l*]pyrene, Dibenzo[*a,i*]pyrene
Dibenzo[*a,e*]pyrene	Dibenzo[*a,e*]pyrene
Dibenzo[*a,i*]pyrene	Dibenzo[*a,i*]pyrene, Dibenzo[*a,l*]pyrene
Benzo[*a*]pyrene tetrol	Benzo[*a*]pyrene tetrol, Dibenzo[*a,e*]pyrene

[a] Matches are given at the 95% probability level.

4. Conclusions

This study demonstrates that current theoretical methods for calculating fluorescent spectra of PAHs are sufficiently accurate that a given experimental spectrum can be correctly matched to a computed spectrum from a statistical comparison to a small library of computed spectra. The compounds chosen here for comparison provide a challenging test case with three isomers of $C_{24}H_{14}$ and a PAH containing heteroatoms. In all cases, the best predictions are obtained when the CAM-B3LYP method is utilized and the influence of solvent is included.

Ultimately, these theoretical methods may prove useful in predicting spectra in cases where commercial standards are unavailable. For example, the analysis of higher molecular weight PAHs (i.e. PAHs > 300 g mol^{-1}) is presently limited by the lack of commercial standards. This is particularly problematic for PAHs with a molecular weight of 302 because such PAHs have been shown to have significant toxicity yet only 23 standards are commercially available for the 88 possible isomers [35]. Obviously, for higher molecular weight PAHs the number of structural isomers increases rapidly and the absence of commercial standards becomes even more pronounced. For this ultimate application, however, more sophisticated methods of identification (e.g. pattern recognition)

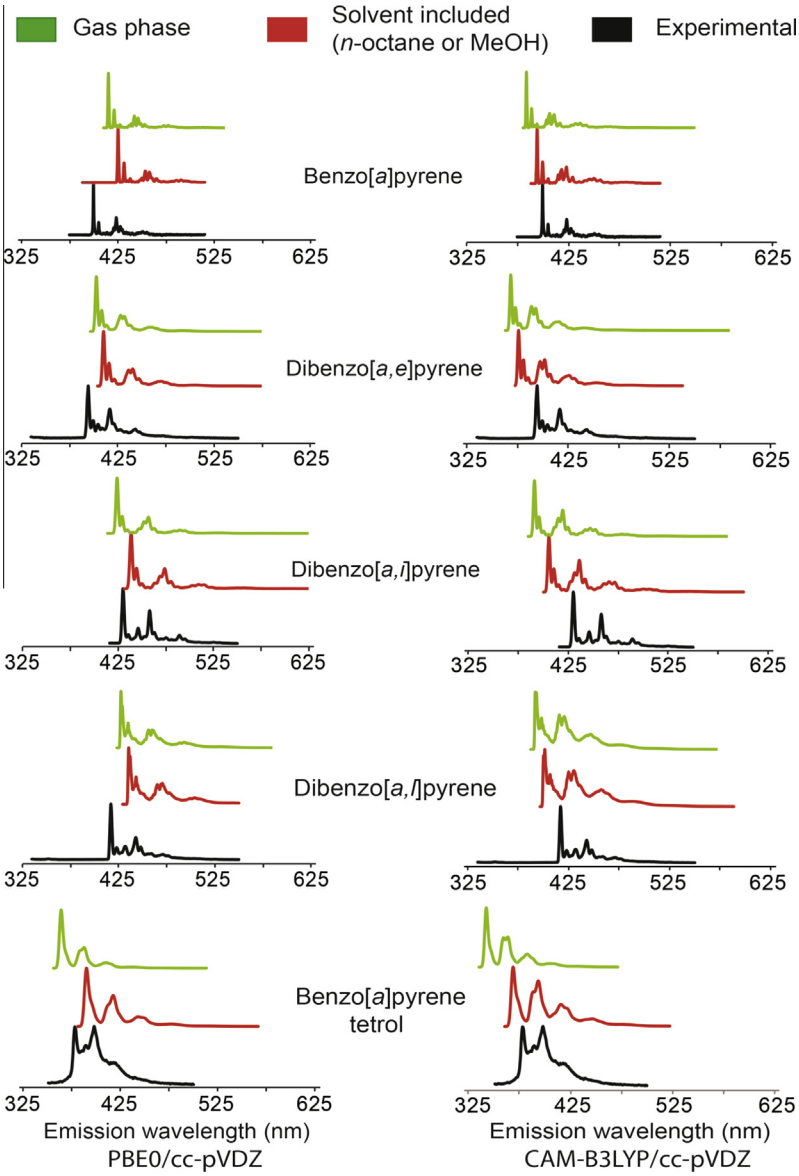

Fig. 9. A plot showing the influence of solvent on DFT predicted spectra of PAHs. Spectra in the left and right columns show, respectively, data computed with the PBE0 and CAM-B3LYP methods. Green, orange and black spectra denote, respectively, spectra calculated in the gas phase, spectra computed with solvent included and experimental data. Most experimental spectra were acquired at 4.2 K in *n*-octane, but the benzo[*a*]pyrene tetrol spectrum was acquired at room temperature in methanol. The computed spectra include either *n*-octane or methanol to match experimental conditions. (For interpretation of the references to color in this figure legend, the reader is referred to the web version of this article.)

would be required – particularly in the case of PAH identification in complex mixtures.

The ability to theoretically predict accurate spectra also provides for the possibility of generating libraries of fluorescent spectra in a digital format. Presently considerable efforts have been devoted to the development of a database of IR spectra for detecting PAHs in space [7,36]. The creation of a comparable database of vibrationally resolved fluorescence spectra for PAHs may be of similar value in pollutant identification. All spectra computed for this study are available as Supplementary Information.

Acknowledgements

We acknowledge the University of Central Florida Stokes Advanced Research Computing Center for providing computational resources and support that have contributed to results reported herein, URL http://webstokes.ist.ucf.edu.

Appendix A. Supplementary material

Supplementary data associated with this article can be found, in the online version, at http://dx.doi.org/10.1016/j.jms.2016.06.015.

References

[1] J.H. Hahn, R. Zenobi, J. Bada, R.N. Zare, Science 239 (1988) 1523.
[2] L.J. Allamandola, S.A. Sandford, B. Wopenka, Science 237 (1987) 56.
[3] L.J. Allamandola, A.G.G.M. Tielens, J.R. Barker, Astrophys. J. 290 (1985) L25.
[4] H. Wu, C. Cao, C.-N. Hao, F.-S. Liu, J.-L. Wang, X.-Y. Xia, Z.-G. Den, C.K.-S. Young, Astrophys. J. 632 (2005) L79.
[5] T. Takahashi, T. Takenobu, J. Takeya, Y. Iwasa, Adv. Funct. Mater. 17 (2007) 1623.
[6] C.W.J. Bauschlicher, A. Ricca, Chem. Phys. Lett. 326 (2000) 283.
[7] L.J. Allamandola, A.G.G.M. Tielens, J.R. Barker, Astrophys. J. Suppl. Ser. 71 (1989) 733.
[8] J.C. Brown, J.A. Duncanson, G. Small, J. Anal. Chem. 52 (1980) 1711.
[9] A.J. Bystol, A.D. Campiglia, G.D. Gillispie, Anal. Chem. 73 (2001) 5762.
[10] T.L. Martin, A.D. Campiglia, Appl. Spectrosc. 55 (2001) 1266.
[11] H. Wang, S. Yu, A.D. Campiglia, Anal. Biochem. 385 (2009) 249.
[12] S. Yu, H.C. Goicoechea, A.D. Campiglia, Appl. Spectrosc. 61 (2007) 165.
[13] C. Gooijer, F. Ariese, J.W. Hofstraat (Eds.), Shpol'skii Spectroscopy and Other Site-Selection Methods: Applications in Environmental Analysis, Bioanalytical Chemistry, and Chemical Physics, John Wiley & Sons, New York, 2000.
[14] A.J. Bystol, T. Thorstenson, A.D. Campiglia, Environ. Sci. Technol. 36 (2002) 4424.
[15] A.F.T. Moore, H.C. Goicoechea, F. Barbosa Jr., A.D. Campiglia, Anal. Chem. 87 (2015) 5232.
[16] P. Schubert, M.M. Schantz, L.C. Sander, S.A. Wise, Anal. Chem. 75 (2003) 234.
[17] (a) V. Barone, J. Bloino, M. Biczysko, F. Santoro, J. Chem. Theory Comput. 5 (2009) 540;
(b) J. Bloino, M. Biczysko, F. Santoro, V. Barone, J. Chem. Theory Comput. 6 (2010) 1256;
(c) R. Improta, V. Barone, F. Santoro, Angew. Chem., Int. Ed. 46 (2007) 405.
[18] P. Hohenberg, W. Kohn, Phys. Rev. 136 (1964) 864.
[19] (a) E.K.U. Gross, J.F. Dobson, M. Petersilka, Top. Curr. Chem. 181 (1996) 81;
(b) R.J. Van Leeuwen, Mod. Phys. B (2001) 1969;
(c) G. Onida, L. Reining, A. Rubio, Rev. Mod. Phys. 74 (2002) 601.
[20] (a) F. Santoro, R. Improta, A. Lami, J. Bloino, V. Barone, J. Chem. Phys. 126 (2007) 084509;
(b) F. Santoro, R. Improta, A. Lami, J. Bloino, V. Barone, J. Chem. Phys. 126 (2007) 184102.
[21] Representative examples include: (a) A. Pedone, J. Bloino, V. Barone, J. Phys. Chem. C 116 (2012) 17807;
(b) N. De Mitri, S. Monti, G. Prampolini, V. Barone, J. Chem. Theory Comput. 9 (2013) 4507.
[22] (a) A.Y. Freidzon, R.R. Valiev, A.A. Brezhnoy, RCS Adv. 4 (2014) 42054;
(b) P. Liu, Z. He, G.-L. Hou, B. Guan, H. Lin, Z. Huang, J. Phys. Chem. C 119 (2015) 13009;
(c) M. Pang, P. Yang, W. Shen, M. Li, R. He, Chem. Phys. Lett. 628 (2015) 35;
(d) M. D'Alessandro, M. Aschi, C. Mazzuca, A. Palleschi, A. Amadei, J. Chem. Phys. 139 (2013) 114102;
(e) A. Charaf-Eddin, A. Planchat, B. Mennucci, C. Adamo, D. Jacquemin, J. Chem. Theory Comput. 9 (2013) 2749;
(f) C.-W. Wang, L. Yang, C. Zhu, J.-G. Yu, S.-H. Lin, J. Chem. Phys. 141 (2014) 084106.
[23] C. Achten, J.T. Andersson, Polycyclic Aromat. Compd. 35 (2015) 177.
[24] J.T. Andersson, C. Achten, Polycyclic Aromat. Compd. 35 (2015) 330.
[25] A.D. Ragin, K.C. Crawford, C. Davies, M. Hallett, A.A. Etheredge, J. Grainger, D.G. Patterson Jr., Polycyclic Aromat. Compd. 28 (2008) 438.
[26] (a) J.P. Perdew, K. Burke, M. Ernzerhof, Phys. Rev. Lett. 77 (1996) 3865;
(b) C. Adamo, V. Barone, J. Chem. Phys. 110 (1999) 6158.
[27] T. Yanai, D. Tew, N. Handy, Chem. Phys. Lett. 393 (2004) 51.
[28] A.D. Campiglia, A.J. Bystol, S. Yu, Anal. Chem. 78 (2006) 484.
[29] T.H. Dunning, J. Chem. Phys. 90 (1989) 1007.
[30] J. Tomasi, B. Mennucci, R. Cammi, Chem. Rev. 105 (2005) 2999.
[31] M.J. Frisch, G.W. Trucks, H.B. Schlegel, G.E. Scuseria, M.A. Robb, J.R. Cheeseman, G. Scalmani, V. Barone, B. Mennucci, G.A. Petersson, H. Nakatsuji, M. Caricato, X. Li, H.P. Hratchian, A.F. Izmaylov, J. Bloino, G. Zheng, J.L. Sonnenberg, M. Hada, M. Ehara, K. Toyota, R. Fukuda, J. Hasegawa, M. Ishida, T. Nakajima, Y. Honda, O. Kitao, H. Nakai, T. Vreven, J.A. Montgomery Jr., J.E. Peralta, F. Ogliaro, M.J. Bearpark, J. Heyd, E.N. Brothers, K.N. Kudin, V.N. Staroverov, R. Kobayashi, J. Normand, K. Raghavachari, A.P. Rendell, J.C. Burant, S.S. Iyengar, J. Tomasi, M. Cossi, N. Rega, N.J. Millam, M. Klene, J.E. Knox, J.B. Cross, V. Bakken, C. Adamo, J. Jaramillo, R. Gomperts, R.E. Stratmann, O. Yazyev, A.J. Austin, R. Cammi, C. Pomelli, J.W. Ochterski, R.L. Martin, K. Morokuma, V.G. Zakrzewski, G.A. Voth, P. Salvador, J.J. Dannenberg, S. Dapprich, A.D. Daniels, Ö. Farkas, J.B. Foresman, J.V. Ortiz, J. Cioslowski, D.J. Fox, Gaussian 09, Revision A.02, Gaussian, Inc., Wallingford, CT, USA, 2009.
[32] (a) M. D'Abramo, M. Aschi, A. Amadei, J. Chem. Phys. 140 (2014) 164104;
(b) F. Santoro, A. Lami, R. Improta, J. Bloino, V. Barone, J. Chem. Phys. 128 (2008) 224311;
(c) N. De Mitri, S. Monti, G. Prampolini, V. Barone, J. Chem. Theory Comput. 9 (2013) 4507.
[33] (a) K. Kalakewich, R. Iuliucci, K.T. Mueller, H. Eloranta, J.K. Harper, J. Chem. Phys. 143 (2015) 194702;
(b) J.K. Harper, R. Iuliucci, C-13 chemical shift tensors in organic materials, in: R.A. Meyers (Ed.), Encyclopedia of Analytical Chemistry, Wiley, New York, 2014, pp. 1–37;
(c) J.K. Harper, D.H. Barich, J.Z. Hu, G.A. Strobel, D.M. Grant, J. Org. Chem. 68 (2003) 4609;
(d) J.K. Harper, J.C. Facelli, D.H. Barich, G. McGeorge, A.E. Mulgrew, D.M. Grant, J. Am. Chem. Soc. 124 (2002) 10589;
(e) J.K. Harper, D.M. Grant, J. Am. Chem. Soc. 122 (2000) 3708;
(f) J.K. Harper, G. McGeorge, D.M. Grant, J. Am. Chem. Soc. 121 (1999) 6488;
(g) J.K. Harper, G. McGeorge, D.M. Grant, Magn. Reson. Chem. 36 (1998) S135;
(h) J.K. Harper, J.A. Doebbler, E. Jacques, D.M. Grant, R. Von Dreele, J. Am. Chem. Soc. 132 (2010) 2928.
[34] K. Varmuza, in: G. Berthier, M.J.S. Dewar, H. Fischer, K. Fukui, G.G. Hall, H. Hartmann, H.H. Jaffe, J. Jortner, W. Kutzelnigg, K. Ruedenburg, E. Scrocco, W. Zeil (Eds.), Lecture Notes in Chemistry: Pattern Recognition in Chemistry, vol. 21, Springer-Verlag, New York, 1980.
[35] National Institute of Standards and Technology (NIST) <http://webbook.nist.gov/chemistry/> (accessed May 6, 2016).
[36] A. Ricca, C.W.J. Bauschlicher, C. Boersma, A.G.G.M. Tielens, L.J. Allamandola, Astrophys. J. 754 (2012) 1.